Supplementary material

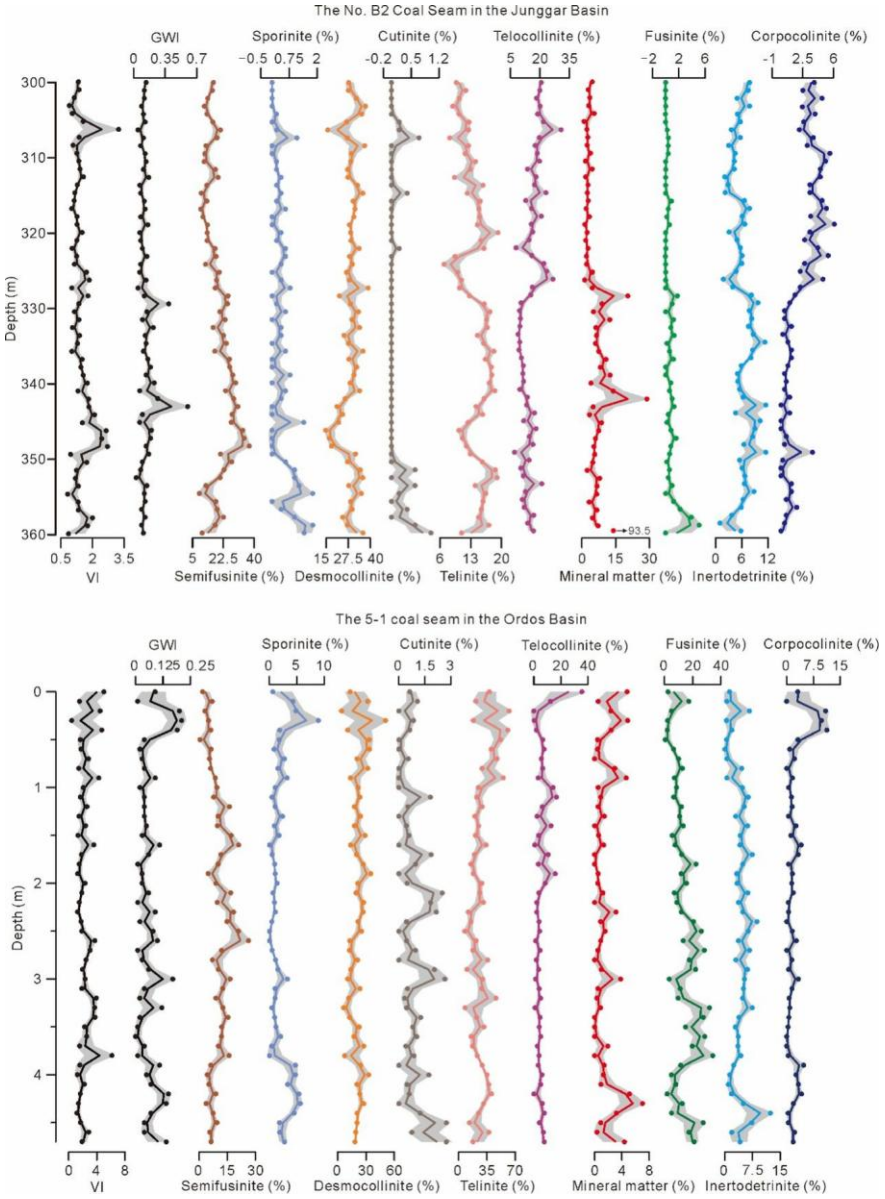


Figure S1. Summary diagram of coal macerals, groundwater index (GWI) and vegetation index (VI) data from the No. B2 coal seam in the Junggar Basin and the No. 5-1 coal seam in the Ordos Basin.

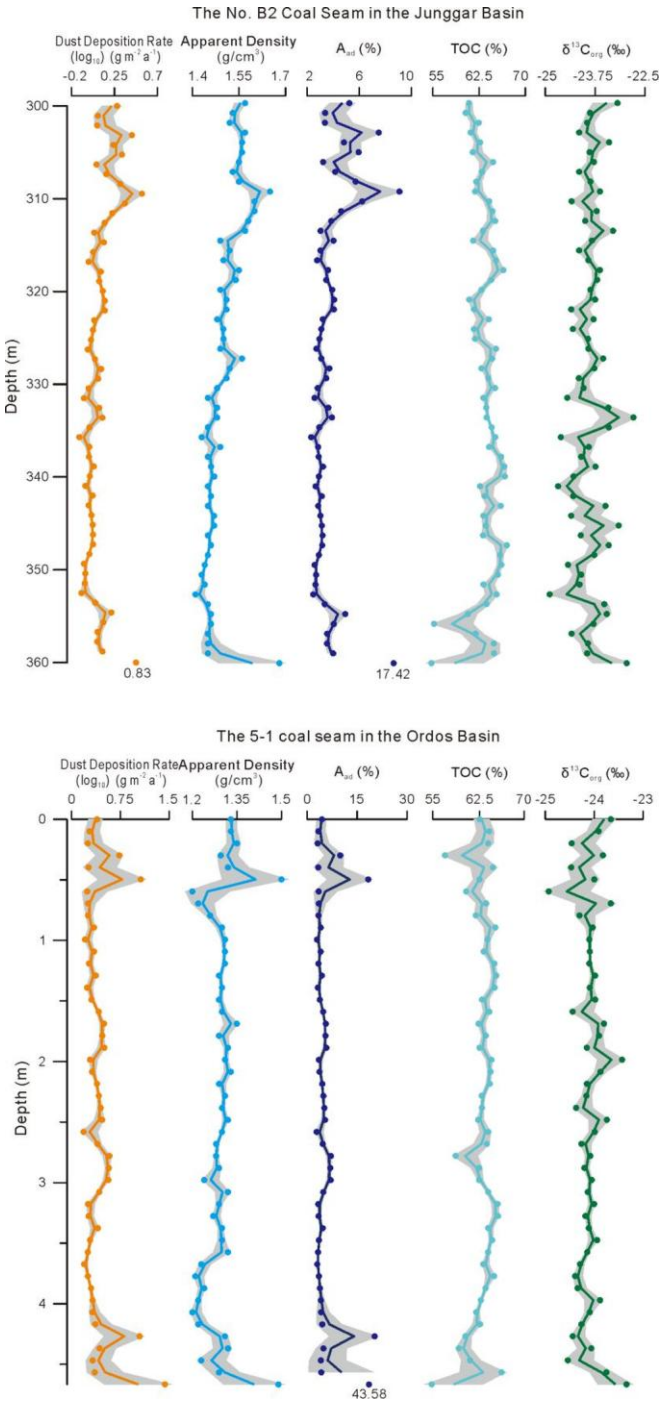


Figure S2. Summary diagram of peatland dust deposition rate, apparent density (ARD), air-dried-basis ash yield (A_{ad}), the total organic carbon (TOC), and bulk organic carbon isotope ($\delta^{13}C_{org}$) from the No. B2 coal seam in the Junggar Basin and the No. 5-1 coal seam in the Ordos Basin.

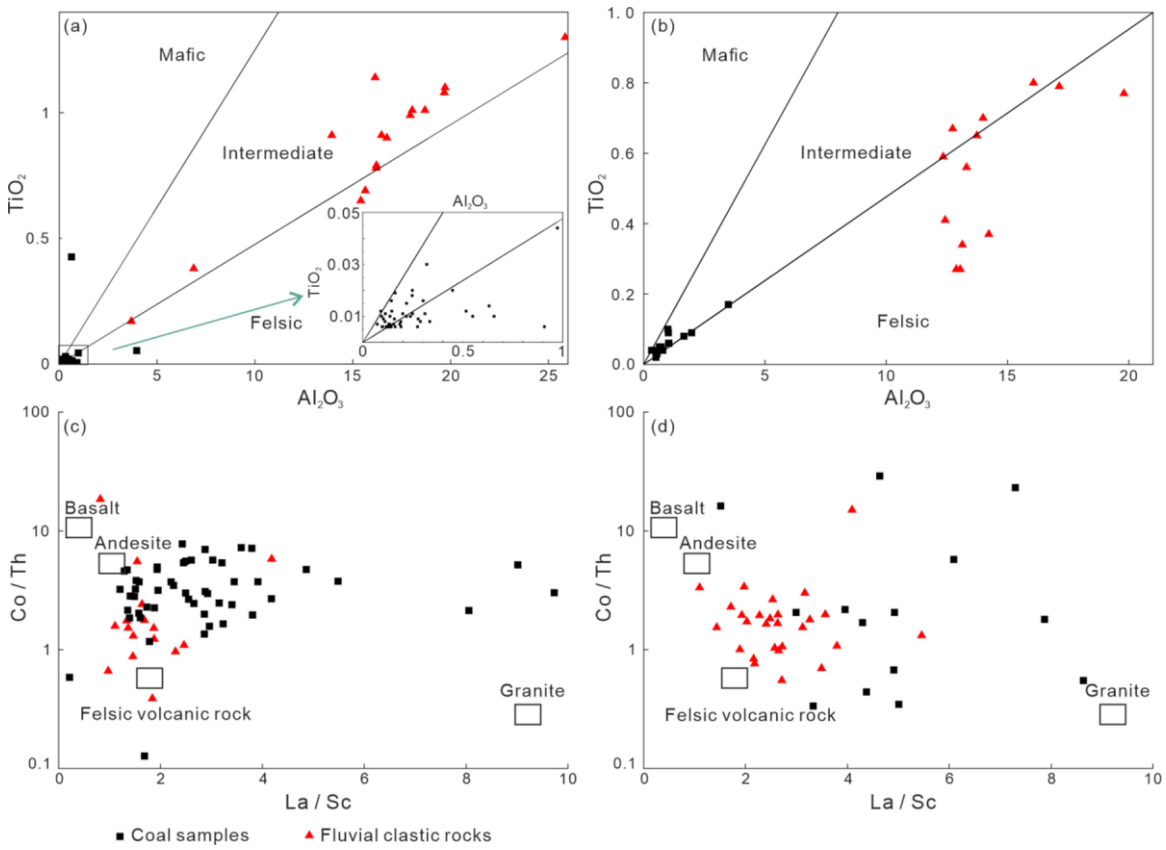


Figure S3. Geochemical provenance comparison between coal samples and published coeval regional clastic rocks from the Middle Jurassic Xishanyao and Yan'an formations. (a, c) Xishanyao Formation, Junggar Basin. (b, d) Yan'an Formation, Ordos Basin. (a, b) Al_2O_3-TiO_2 discrimination diagrams showing mafic-, intermediate-, and felsic-source affinities. (c, d) La/Sc versus Co/Th diagrams. Geochemical data for the Xishanyao coal samples are from this study, whereas data for the Yan'an coal samples are from L. Wang et al. (2022). Published clastic-rock data for the Xishanyao Formation are from Wang et al. (2024); major-element data for the Yan'an Formation are from Bai et al. (2025); trace-element data for the Yan'an Formation are from Y. Li et al. (2022). Reference compositions for basalt, andesite, felsic volcanic rocks, and granite are from Gu et al. (2002); classification boundaries in the Al_2O_3-TiO_2 diagrams are after Hayashi et al. (1997).

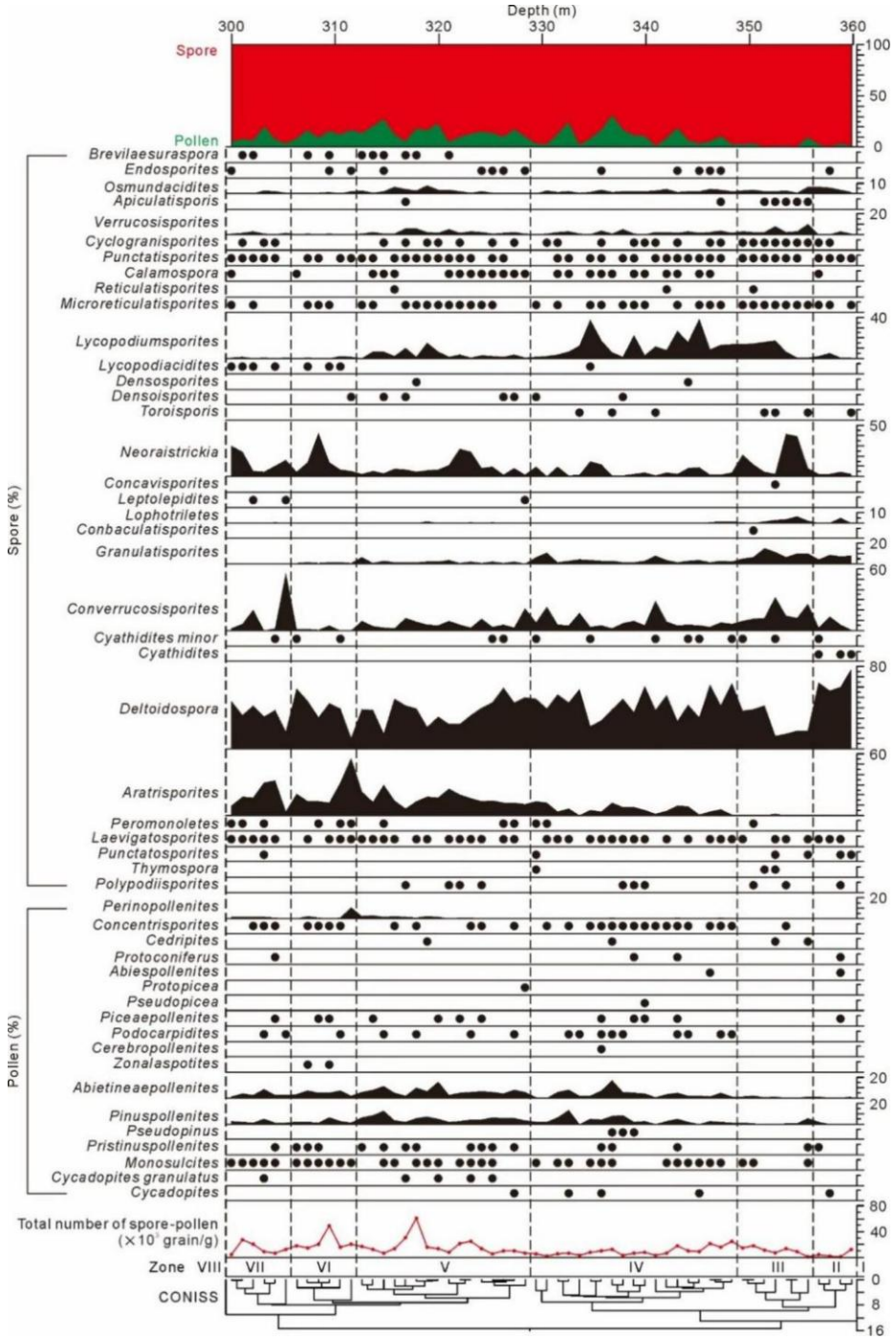


Figure S4. Quantitative distribution of spore-pollen taxa from the No. B2 coal seam in the Junggar Basin. Palynomorph abundance values are presented as percentage proportions (%) of the total spore-pollen sum. For rare taxa (abundance less than 5 counts per sample) only presence-absence data are shown (black circles).

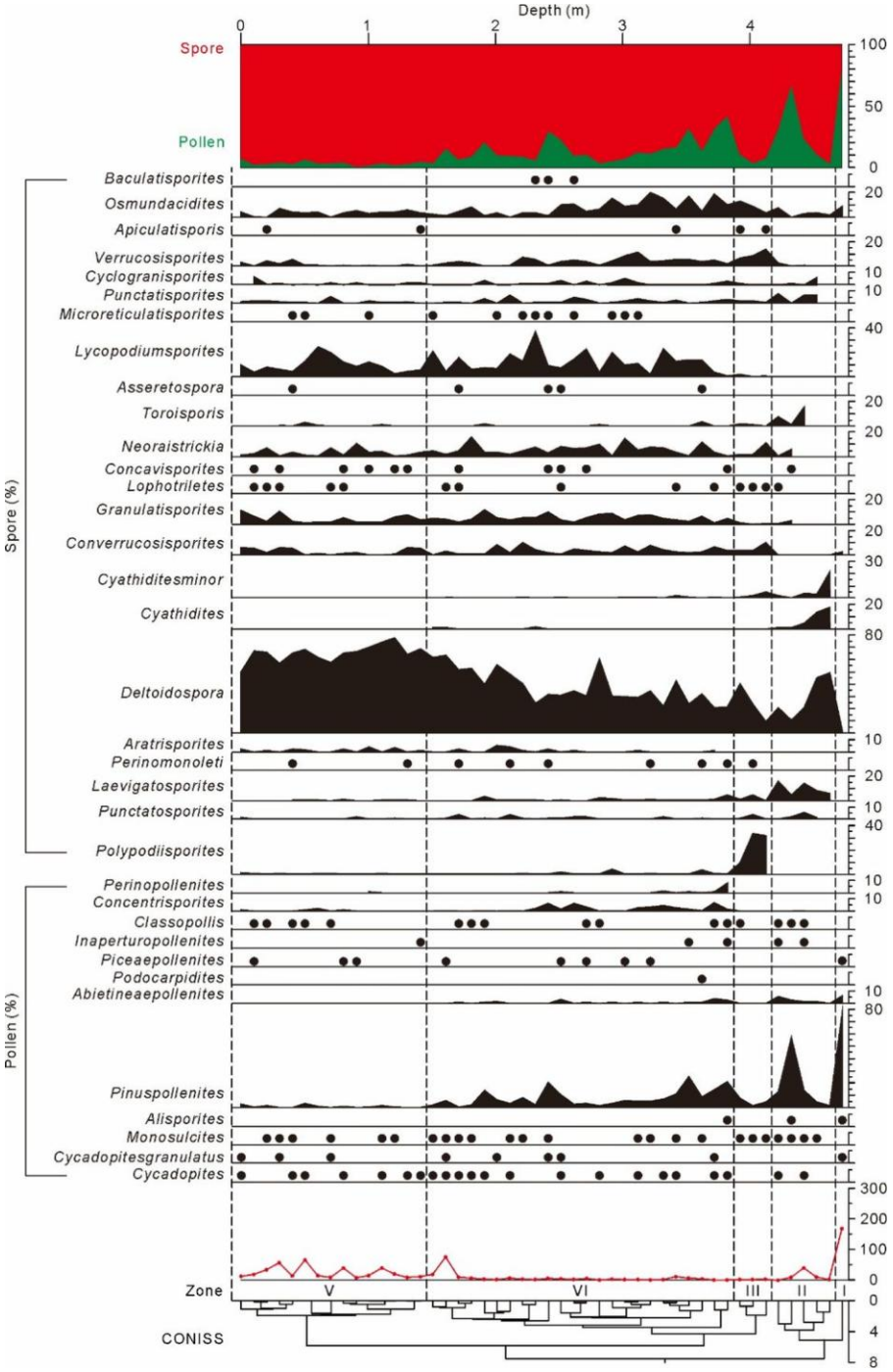


Figure S5. Quantitative distribution of spore-pollen taxa from the No. 5-1 coal seam in the Ordos Basin. Palynomorph abundance values are presented as percentage proportions (%) of the total spore-pollen sum. For rare taxa (abundance <5 counts per sample) only presence-absence data are shown (black circles).

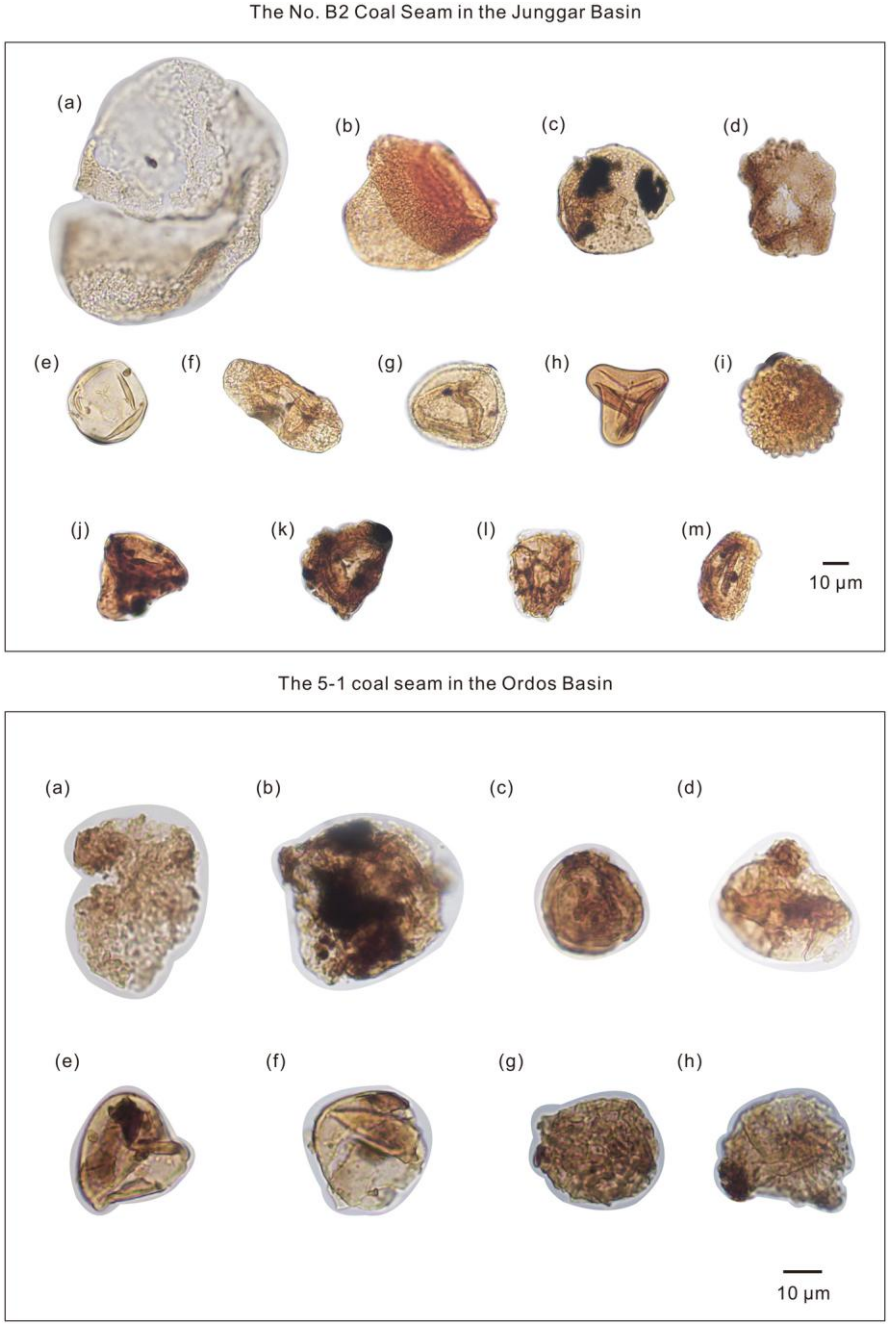


Figure S6. Selected plant spore-pollen taxa from the No. B2 coal seam in the Junggar Basin and the No. 5-1 coal seam in the Ordos Basin. The Junggar Basin: (a) *Piceaepollenites;* (b) *Podocarpidites;* (c) *Osmundacidites;* (d) *Abietineaepollenites;* (e) *Calamospora;* (f) *Pinuspollenites;* (g) *Densoisporites;* (h) *Cyathidites;* (i) *Cerebropollenites;* (j) *Toroisporis;* (k) *Endosporites;* (l) *Lycopodiumsporites;* (m) *Aratrisporites;* The Ordos Basin: (a) *Pinuspollenites;* (b) *Abietineaepollenites;* (c) *Classopollis;* (d) *Aratrisporites;* (e) *Toroisporis;* (f) *Cyathidites;* (g) *Lycopodiumsporites;* (h) *Osmundacidites.*

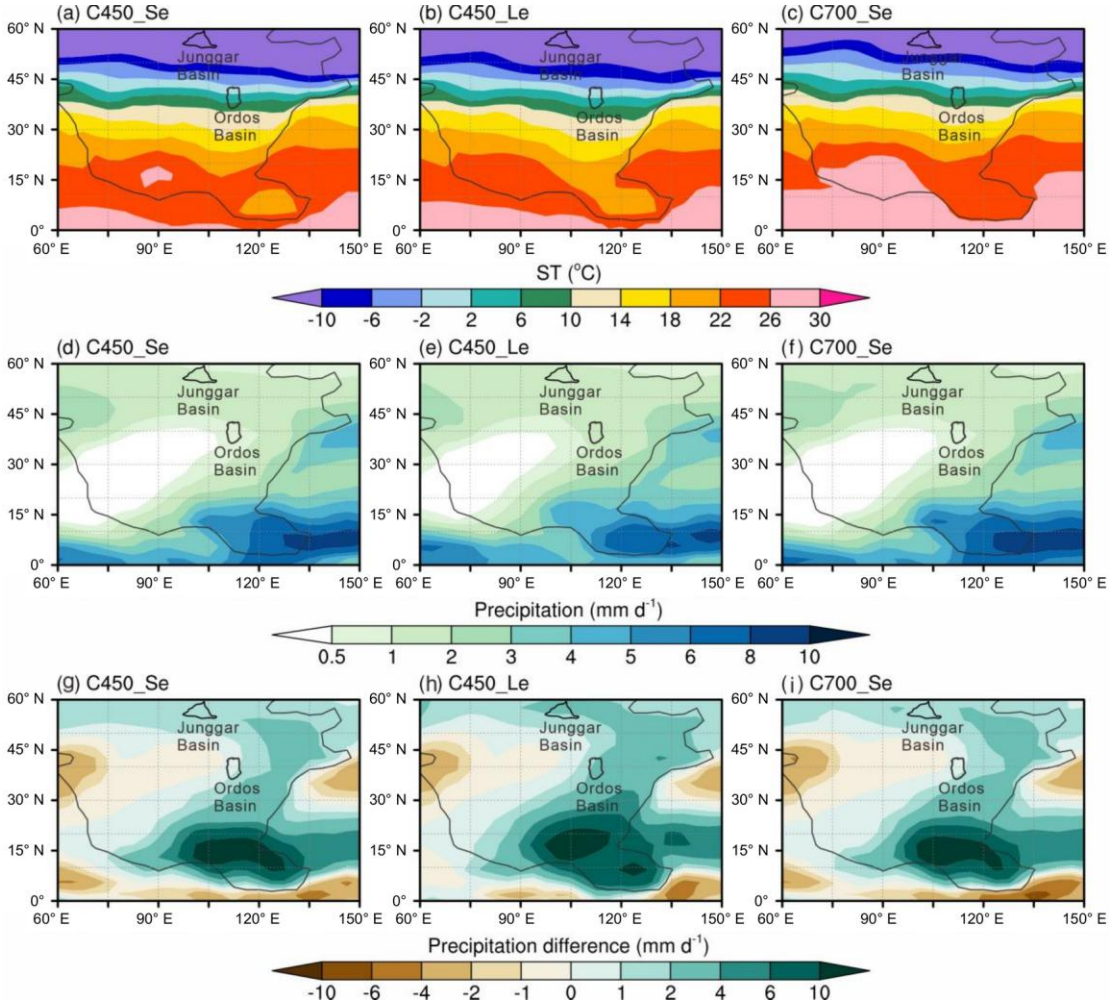


Figure S7. Simulated regional Northern Hemisphere surface temperature, precipitation, and summer-winter precipitation difference under different eccentricity and pCO_2 scenarios during the Middle Jurassic. (a–c) Surface temperature (ST), (d–f) precipitation, and (g–i) summer-winter precipitation difference, calculated as mean June–August precipitation minus mean November–January precipitation, for experiments C450_Se, C450_Le, and C700_Se, respectively. C450 and C700 denote pCO_2 levels of 450 and 700 ppmv, respectively; Le and Se denote high- and low-eccentricity conditions, respectively.

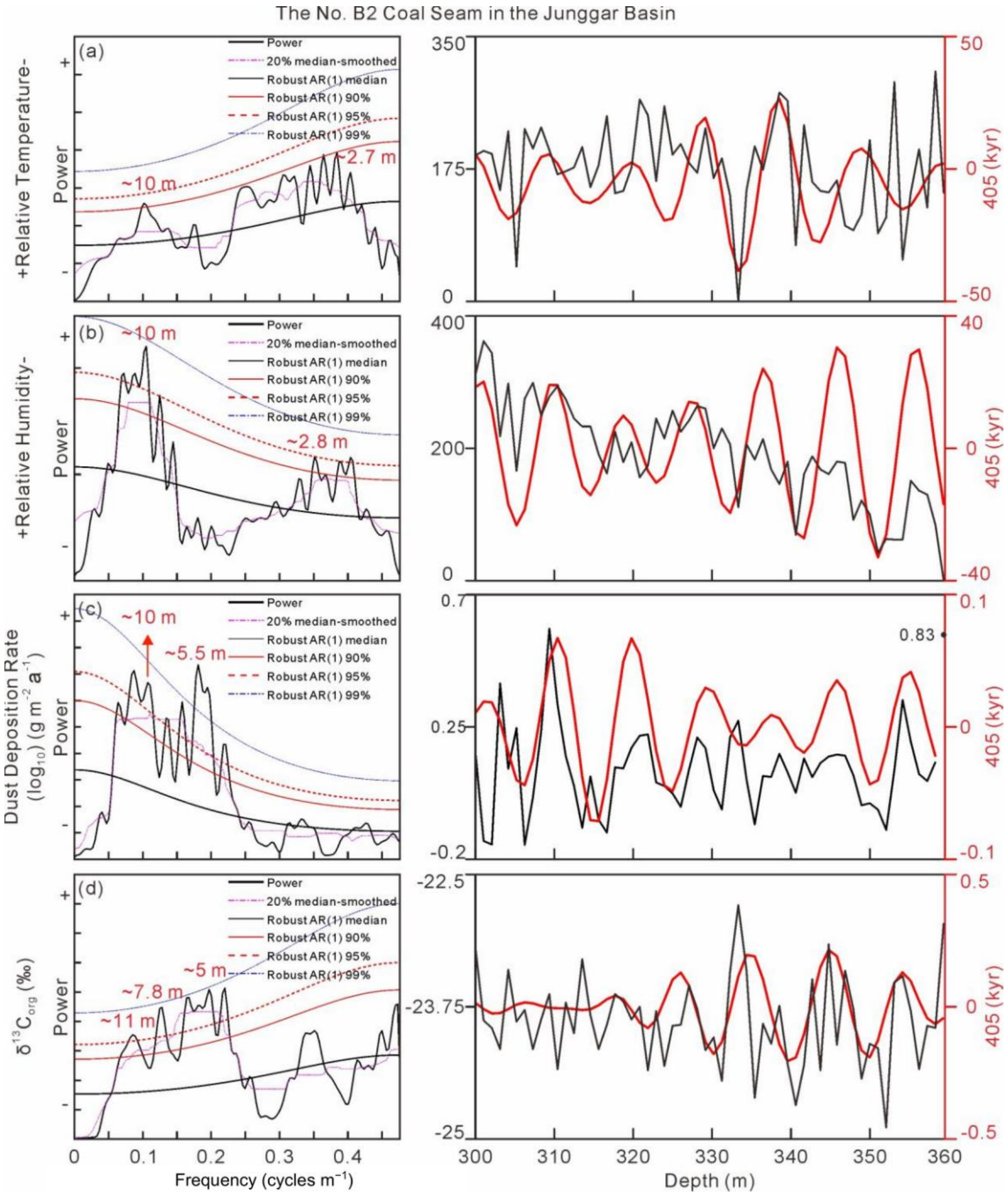
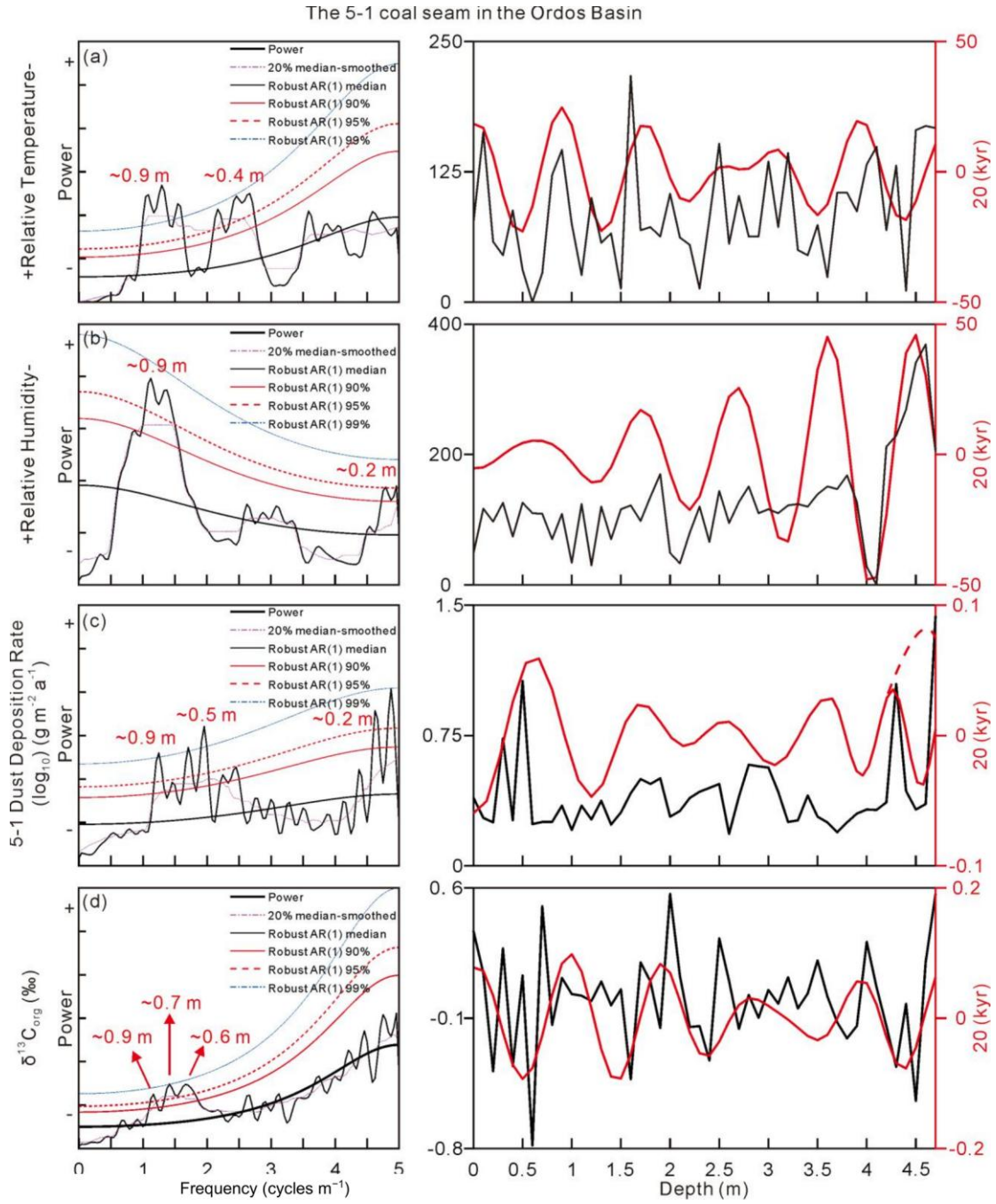


Figure S8. Analysis of astronomical orbital cyclic signals of data series (black curves on the right) from the No. B2 coal seam in the Junggar Basin (a–d: DCA temperature-related axis scores, DCA humidity-related axis scores, dust deposition rates in peatland and $\delta^{13}C_{org}$). 2π or 3π multi-taper method (MTM) power spectrum of the data series after removing the 35 % LOWESS trend. Gaussian band-pass filtering (passband: 0.11 ± 0.02 cycles m^{-1}) isolates ~10 m component, corresponding to ~405 kyr under the adopted astrochronologic framework.



45 **Figure S9. Analysis of astronomical orbital cyclic signals of data series (black curves on the right) from the No. 5-1 coal seam in the Ordos Basin (a–d: DCA temperature-related axis scores, DCA humidity-related axis scores, dust deposition rates in peatland and $\delta^{13}C_{org}$). 2π or 2.5π multi-taper method (MTM) power spectrum of the data series after removing the 35 % LOWESS trend. Gaussian band-pass filtering (passband: 1.11 ± 0.22 cycles m^{-1}) isolates a ~0.9 m component, corresponding to ~20 kyr under the adopted astrochronologic framework.**

Table S1. Description of the Middle Jurassic paleoclimate modeling experiments

Experiment	pCO_2 (ppmv)	Eccentricity	Longitude of perihelion (°)	Obliquity
C450_Se	450	0.0066	270	23.45°
C450_Le	450	0.066	270	23.45°
C700_Se	700	0.0066	270	23.45°

References

Bai, Y., Liu, B., and Li, H.: Geochemical characteristics of green sandstones in Mesozoic uranium-bearing strata in the northern Ordos Basin and their implications, Uranium Geol., 41, 13–28, (in Chinese with English abstract), https://doi.org/10.3969/j.issn.1000-0658.2025.41.002, 2025.

Gu, X. X., Liu, J. M., Zheng, M. H., Tang, J. X., and Qi, L.: Provenance and tectonic setting of the Proterozoic turbidites in Hunan, South China: Geochemical evidence, J. Sediment. Res., 72, 393–407, https://doi.org/10.1306/081601720393, 2002.

Hayashi, K.-I., Fujisawa, H., Holland, H. D., and Ohmoto, H.: Geochemistry of ~1.9 Ga sedimentary rocks from northeastern Labrador, Canada, Geochim. Cosmochim. Acta, 61, 4115–4137, https://doi.org/10.1016/S0016-7037(97)00214-7, 1997.

Li, Y., Yan, M., Liu, P., Lin, H., Li, S., Huo, S., and Yang, T.: Characteristics of the tectonic background and sedimentary paleoenvironment of coal-bearing strata from the Yan'an Formation in the Ordos Basin: Evidence from the geochemistry of major and trace elements, ACS Earth Space Chem., 6, 2680–2697, https://doi.org/10.1021/acsearthspacechem.2c00240, 2022.

Wang, L., Lv, D., Hower, J. C., Zhang, Z., Raji, M., Tang, J., Liu, Y., and Gao, J.: Geochemical characteristics and paleoclimate implication of Middle Jurassic coal in the Ordos Basin, China, Ore Geol. Rev., 144, 104848, https://doi.org/10.1016/j.oregeorev.2022.104848, 2022.

Wang, Y., Wang, W., Wang, W., and Duan, P.: Geochemical characteristics and sedimentary paleoenvironment of the coal-bearing strata in the Xishanyao Formation: A case study of the Yihua Coal Mine in the Zhundong Coalfield, Xinjiang, Minerals, 14, 461, https://doi.org/10.3390/min14050461, 2024.